Published in : Astrophysics and Space Science (2022), vol. 367, n°123
DOI: 10.1007/s10509-022-04142-6
Status : Postprint (Author's version)

UNDERSTANDING STRUCTURE IN LINE-DRIVEN STELLAR WINDS USING ULTRAVIOLET SPECTROPOLARIMETRY IN THE TIME DOMAIN

Kenneth G. Gayley[1], Jorick S. Vink[2], Asif ud-Doula[3], Alexandre David-Uraz[4,5], Richard Ignace[6], Raman Prinja[7], Nicole St-Louis[8], Sylvia Ekström[9], Yaël Nazé[10], Tomer Shenar[11], Paul A. Scowen[12], Natallia Sudnik[13], Stan P. Owocki[14], Jon O. Sundqvist[15], Florian A. Driessen[15], Levin Hennicker[15]

[1] *Department of Physics and Astronomy, University of Iowa, Iowa City, IA, 52242, USA*
[2] *Armagh Observatory and Planetarium, College Hill, BT65 9DG Armagh, Northern Ireland, UK*
[3] *Penn State Scranton, 120 Ridge View Drive, Dunmore, PA 18512, USA*
[4] *Department of Physics and Astronomy, Howard University, Washington, DC 20059, USA*
[5] *Center for Research and Exploration in Space Science and Technology, and X-ray Astrophysics Laboratory, NASA/GSFC, Greenbelt, MD 20771, USA*
[6] *Department of Physics & Astronomy, East Tennessee State University, Johnson City, TN 37614, USA*
[7] *Department of Physics and Astronomy, University College London, Gower Street, London WC1E 6BT, UK*
[8] *Département de physique, Université de Montréal, Complexe des Sciences, 1375 Avenue Thérèse-Lavoie-Roux, Montréal (QC), H2V 0B3, Canada*
[9] *Department of Astronomy, University of Geneva, Chemin Pegasi 51, 1290 Versoix GE, Switzerland*
[10] *GAPHE, Univ. of Liège, B5C, Allée du 6 Août 19c, B-4000 Liège, Belgium*
[11] *Anton Pannekoek Institute for Astronomy and Astrophysics, University of Amsterdam, 1090 GE Amsterdam, The Netherlands*
[12] *NASA/GSFC, Greenbelt, MD 20771, USA*
[13] *Nicolaus Copernicus Astronomical Centre of the Polish Academy of Sciences, Bartycka 18, 00-716 Warsaw, Poland*
[14] *Department of Physics and Astronomy, University of Delaware, 217 Sharp Lab, Newark, DE, USA*
[15] *Institute of Astronomy, KU Leuven, Celestijnenlaan 200D/2401, 3001 Leuven, Belgium*

KEYWORDS: *Polstar* – NASAMIDEX ; Far ultraviolet ; Near ultraviolet astronomical observations ; Extreme ultraviolet astronomy ; Spectropolarimetry ; Explorer ; Massive stars ; Stellar rotation

ABSTRACT

The most massive stars are thought to lose a significant fraction of their mass in a steady wind during the main-sequence and blue supergiant phases. This in turn sets the stage for their further evolution and eventual supernova, and preconditions the surrounding medium for all following events, with consequences for ISM energization, chemical enrichment, and dust formation. Understanding these processes requires accurate observational constraints on the mass-loss rates of the most luminous stars, which can also be used to test theories of stellar wind driving. In the past, mass-loss rates have been characterized via collisional emission processes such as optical H and free-free radio emission, but these so-called "density squared" diagnostics require correction in the presence of widespread clumping. Recent observational and theoretical evidence points to the likelihood of a ubiquitously high level of such clumping in hot-star winds, but quantifying its effects requires a deeper understanding of the complex dynamics of radiatively driven winds and their stochastic instabilities.

Published in : Astrophysics and Space Science (2022), vol. 367, n°123
DOI: 10.1007/s10509-022-04142-6
Status : Postprint (Author's version)

Furthermore, large-scale structures initiating in surface anisotropies and propagating throughout the wind can also affect wind driving and alter mass-loss diagnostics. Time series spectroscopy of high resonance-line opacity in the UV, capable of high resolution and high signal-to-noise, are required to better understand these complex dynamics, and more accurately determine mass-loss rates. The proposed *Polstar* mission (Scowen et al. 2022, this volume) provides the necessary resolution at the Sobolev (~10 km s^{-1}) or sound-speed (~20 km s^{-1}) scale, for over three dozen bright galactic massive stars with signal-to noise an order of magnitude above that of the celebrated MEGA campaign (Massa et al. 1995) of the International Ultraviolet Explorer (IUE), via continuous observations that track propagating structures through the winds in real time. Supporting geometric constraints are provided by the polarimetric capabilities present in all the datasets of such a mission.

1. Introduction

Theoretical models of the UV line-driven winds of hot stars (Owocki et al. 1988; Feldmeier et al. 1997) have long predicted that internal instabilities should produce high-density clumps and low-density voids, as the hypersonic acceleration cannot be maintained smoothly. Also, in CAK theory (Castor et al. 1975), the acceleration of the wind depends nonlinearly on the mass flux, so variations in the mass flux launched from the stellar photosphere also produce significant velocity and density variations as the wind accelerates. Recent work shows that both these types of wind perturbations quickly steepen into shocks, compressing and driving dense clumps (Sundqvist et al. 2018), and producing observable hard X-ray emission (e.g., Oskinova 2016 and references therein).

Observational evidence that this is occurring already exists in optical emission lines of dense winds, even in single stars. This is seen directly in moving emission bumps (e.g., Moffat et al. 1988; Lépine and Moffat 1999), and indirectly from reduced levels of free-electron scattering in the line wings (Hillier 1991; Hamann and Koesterke 1998). For all these reasons, the idealization of a constant mass-flux, smoothly accelerating hypersonic flow needs to be replaced by a more complete description, to understand actual winds and quantify their influences.

Other factors can also break the spherical symmetry of simple models, including rapid rotation and magnetic fields. It has long been known (Morton 1976; Snow and Morton 1976) that hot-star wind effects are more widely apparent in ultraviolet (UV) rather than optical spectra, so we wish to investigate how all these geometric features affect the shape of UV P Cygni profiles. However, ambiguities persist in purely spectroscopic investigations. Hence this information must be complemented by time dependence and polarization, all of which are accessible to UV spectropolarimetry with continuous observation in the time domain, the focus of this article.

Currently lacking this more complete information, most empirical analyses of stellar atmospheres and winds rely on spherical non-LTE model atmospheres. At the present state of the art, the stellar and wind parameters (including the mass-loss rate $\dot{M}$) are derived by fitting resonance and recombination lines simultaneously. P Cygni lines (often high opacity UV lines such as C iv) are predominately used to determine terminal wind velocities v_∞ (e.g. Prinja et al. 1990), whereas $\dot{M}$ in

Published in : Astrophysics and Space Science (2022), vol. 367, n°123
DOI: 10.1007/s10509-022-04142-6
Status : Postprint (Author's version)

the stronger winds of O-stars (mass-loss rates above 10^{-7} $M_{\odot}$ yr^{-1}, e.g., Mokiem et al. 2007) is often inferred using Hα emission. The latter benefits from arising from what is incontrovertibly the dominant wind species in hot main-sequence stars, ionized H (e.g. Puls et al. 1996).

Yet there is a notable difference between UV resonance lines and (optical) recombination lines such as Hα, since resonance lines are typically dominated by pre-existing UV stellar continuum scattered by optical depth $\propto \rho$, while recombination involves photon creation by binary collisions of particles, thereby producing a flux per volume $\propto \rho^2$. The latter also holds for the free-free radio continuum, so crucial indicators of global wind mass-loss rates are sensitive to the local density variations induced by clumping. Thus, use of these "density squared" diagnostics allow inhomogeneities to mimic a *higher* mass-loss rate.

On the other hand, resonance-line diagnostics can be affected in the opposite sense, mimicking a *lower* mass flux, since clumping can increase photon escape through low-density pockets. Also, the gas in these low-density regions would experience reduced self-shadowing within the lines, enhancing local acceleration and inducing a steeper velocity gradient, further reducing line absorption and exacerbating the shortfall in the inferred mass flux. Hence, obtaining agreement between these various diagnostics requires a better understanding of small-scale wind clumping.

Moreover, the contrasts between these analysis techniques in the UV and optical only offer an opportunity to probe the clumping when both sets of observations are available. This combination is especially powerful when observing simultaneous line profile variations in real time, and when complemented with geometric constraints from concurrent polarization measurements.

Of particular significance for our understanding of wind dynamics and evolutionary consequences of mass loss is stars on the main sequence. That is the longest-lived phase of stellar evolution and the one that happens first, initializing the conditions for all subsequent evolutionary phases–including the ultimate supernova of the massive star. The high-mass end of the main sequence has the most profound impact on galactic evolution because it reprocesses the stellar material much more rapidly than lower-mass stars, and conditions the stellar environment into which photoionization and supernova energization proceed, even leading to formation of the rest of the stellar population. Thus, to understand the role of massive stars on population synthesis in our galaxy and others, we must first accurately determine the mass lost in these decisive initial phases (Langer 2012), and track it through the blue supergiant phase that sets the stage for potentially unstable and eruptive behavior later on.

Despite the clear and present need for clumping corrections to inferred mass-loss rates, high signal-to-noise ratio (SNR) dynamic spectra of hot-star winds are currently rare, and have not been systematically extended across a wide array of stellar types and conditions. The IUE MEGA campaign (Massa et al. 1995) was an excellent first step, but only attained SNR 20-25, and only on a few targets. The efforts by HST were also limited to a few targets, with some hampered by pointing difficulties (Heap 1994), and others by interruptions in the continuous data stream (such as for recent observations of ζ Oph). These experiments detailed the nature of large-scale "discrete absorption component" (DAC) structures that are often seen in massive-star winds (Kaper et al. 1997), but could only hint at a hierarchy of smaller-scale structures, possibly penetrating all the way down to the

Published in : Astrophysics and Space Science (2022), vol. 367, n°123
DOI: 10.1007/s10509-022-04142-6
Status : Postprint (Author's version)

Sobolev scale (~10 km s^{-1}). It thus remains unclear the true nature of the prolific velocity and density variations necessary to account for the weakening of P V absorption (Fullerton et al. 2006) and the absence of free-electron scattering wings in dense winds (Hillier 1991).

One approach to resolving this mystery involves deploying a high-resolution medium-aperture UV spectropolarimetry satellite in a continuous viewing mode, for several days spent on each of 40 bright galactic massive stars over a range of masses and OB spectral types. This would allow monitoring wind clumping and other structures as they develop in real time, while tracking correlated polarimetric variations. The fundamental physics of the wind driving is informed by the nature of stochastic clumping, as well as larger and more coherent structures such as co-rotating interactions regions (CIRs, cf. Mullan 1986; Cranmer and Owocki 1996) and prolate/oblate asphericities.

Such detailed mapping would also allow better corrections to clumping-sensitive mass-loss rate determinations, such as free-free radio (Lamers and Leitherer 1993) and Hα emission (Puls et al. 1996). The importance of such corrections is shown in Fig. 1, which presents the evolution of 60 $M_{\odot}$ models computed until the end of central carbon burning, and shows how this evolution is altered when main-sequence mass-loss rates (chosen from Vink et al. 2001) are reduced by a factor of 2 or 3. The significance of these differences imply that steady mass-loss rates in massive stars need to be quantified to much better than a factor of 2, or the subsequent behavior of the star cannot be accurately predicted.

The differences seen in Fig. 1 are mainly due to the way stronger winds during the main sequence (MS) reduce the size of the core. At the middle of the MS, the $\dot{M}/2$ model has a core that is 3% larger than the standard model, and the $\dot{M}/3$ has a core that is 5% larger. In the middle of central helium burning, the difference increases, amounting to 50% and 45% respectively. At the end of central C-burning, the CO-core mass (M_{CO}) is 57% (35%) larger in the $\dot{M}/2$ ($\dot{M}/3$) models respectively, leading to very different endpoints.

A direct effect of changing the mass-loss rates is the duration of the Wolf-Rayet (WR) phase expected for the models. The standard model becomes a WR star early in the He-burning phase ($X(^4\mathrm{He}) = 0.97$), while the lower $\dot{M}$-rates models arrive later in this regime ($X(^4\mathrm{He}) = 0.29$ and 0.44 respectively). This affects directly their statistical prevalence.

Surprisingly, the models show that the behaviour is not simply monotonic with the reduction factor on the mass-loss rates, revealing the sensitivity of the advanced phases to what precedes them. In stars, gravity and fusion interact in complex ways, and changing one parameter in the modeling feeds back on all other aspects. Because of its high luminosity at the end of the MS, the $\dot{M}/3$ model loses more mass during the crossing of the Hertzsprung-Russell diagram, spends less time with a $\log(T_{\mathrm{eff}}) < 4.0$, and ends its evolution in an intermediate situation between the standard and the $\dot{M}/2$ models.

Hence, changes to mass-loss rates at the factor 2 level can profoundly alter the initial conditions for all subsequent evolution, ultimately changing the final state where supernova occurs. Since internal structure at all scales can induce such changes in the mass-loss rates inferred from Hα and radio

Published in : Astrophysics and Space Science (2022), vol. 367, n°123
DOI: 10.1007/s10509-022-04142-6
Status : Postprint (Author's version)

emissions, understanding high-mass stellar evolution requires resolving and analyzing the dynamical nature of wind clumping.

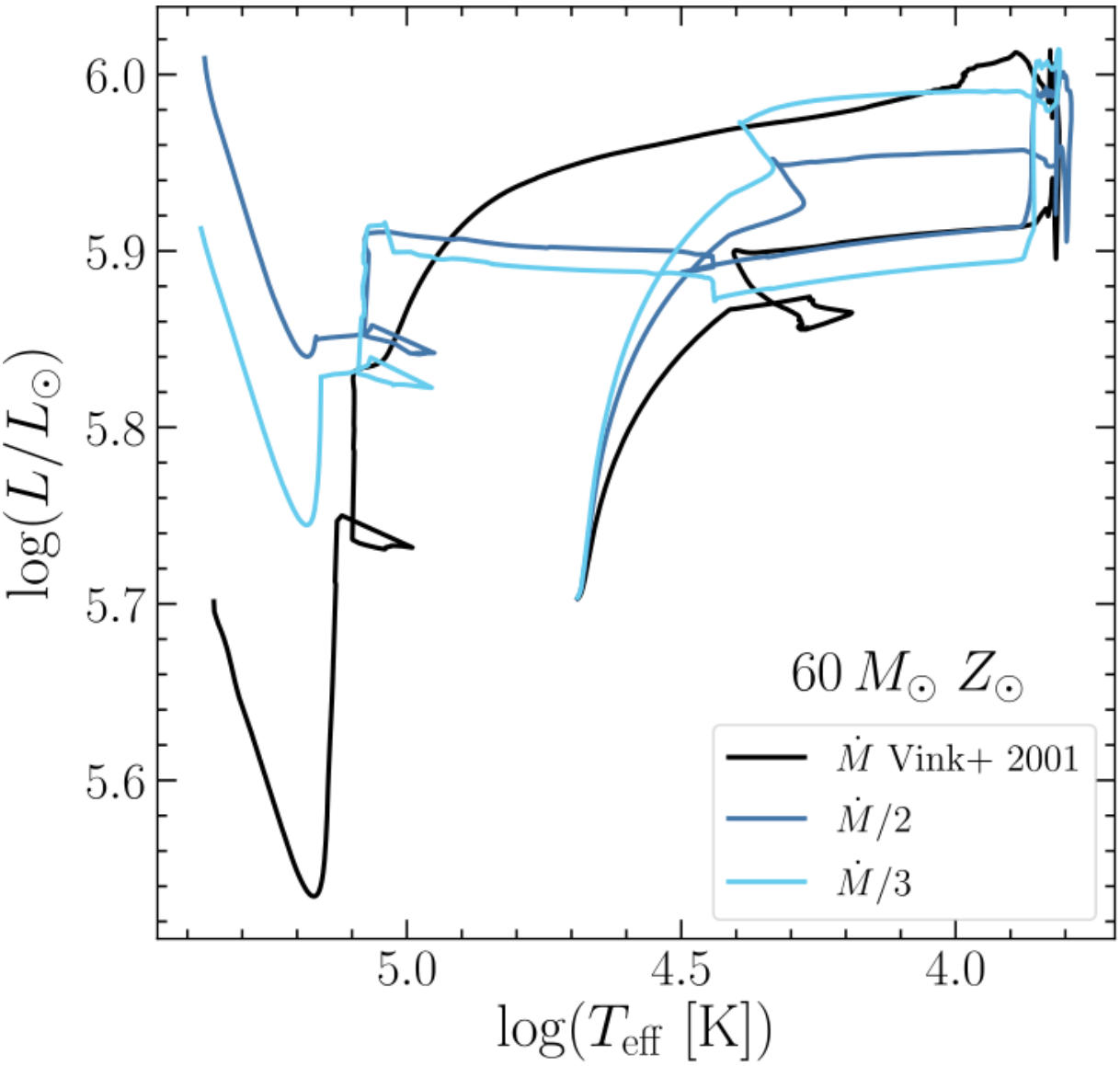

Fig. 1 Hertzsprung-Russell diagram of 60 $M_\odot$ models computed with mass-loss recipe of Vink et al. (2001, black), and the same recipe divided by a factor of 2 and 3 during the MS (teal blue and cyan, respectively)

2. Dynamic spectra

Here we show that MIDEX-class effective area *A* approaching 100 cm^{-2} (and the proposed *Polstar* satellite has a 20-100 cm^{-2} effective area in its high-resolution Channel 1) are well optimized for multiple-day continuous dynamic spectra, suitable for tracking features that slowly accelerate at *a* ≅ 0.02 km s^{-1}, inferred from Massa and Prinja (2015) and Cranmer et al. (2000). This acceleration manifests as changes in the Doppler shifts of features that propagate through the spectral lines, and

Published in : Astrophysics and Space Science (2022), vol. 367, n°123
DOI: 10.1007/s10509-022-04142-6
Status : Postprint (Author's version)

has been seen to persist for many dynamical times, covering several recurrence periods in cases of stellar oscillation or rapid rotation.

To resolve the thermal Doppler scale of metal resonance lines, of order 10 km s^{-1}, and well resolve the wind sound speed of order 20 km s^{-1}, requires a resolution near R = 30,000. Hence we define characteristic resolution $R_{30} = R/(3 \times 10^4)$ and spectral feature acceleration $a_2 = a/(.02$ km $s^{-1})$, and we require an exposure time $t = c/(a\ R)$ to track these features as they accelerate through each resolution element. Hence the intended experiment requires dynamic spectra using exposure time $t = 500/(a_2 R_{30})$ s, for many exposures during continuous monitoring over a timescale of days, in order to follow the features through many dynamical timescales, and potentially also through multiple periods of oscillation and rapid rotation.

To explore the signal-to-noise ratio ($S\,N\,R$) achievable with effective area $A_{100} = A/100$ cm^2, we identify a characteristic UV wavelength of 150 nm and scale all wavelengths via $\lambda_{150} = \lambda/150$ nm, and scale all incident fluxes F at that wavelength via $F_9 = F/10^{-9}$ erg cm^{-1} s^{-1} nm^{-1}, since $F_9 > 1$ includes hundreds of galactic massive-star targets. These definitions give the general result for the signal-to-noise ratio ($S\,N\,R$) for the above exposure time in the relevant limit of pure shot noise (i.e., the square root of counts per resolution element) :

$$SNR = 137 \frac{\lambda_{150}}{R_{30}} \sqrt{\frac{A_{100}}{a_2}} \sqrt{F_9}. \quad (1)$$

This expression can be used to motivate a desirable effective area A_{100} once the desired $S\,N\,R \gg 1$ level is specified.

To reveal small-scale structures at suitably high fidelity to dig significantly deeper than the $S\,N\,R \cong 20 - 25$ typical of dynamic spectra from IUE (Massa and Prinja 2015), HST-accessible $S\,N\,R > 300$ (Cranmer et al. 2000) is desired. Hence we choose a minimum sensitivity of $S\,N\,R = 400$ to achieve positive margin on that goal, a sensitivity deemed necessary to penetrate the full range of the dynamical structures down to the spatial Sobolev scale $\cong r/100$ for radius r. At that scale, we expect ~ 100^2 cross sections of Sobolev size across the face of the star, with a statistical variance of some 1 %, requiring $S\,N\,R$ at the several-hundred level to quantify.

Hence if we define $S\,N\,R_{400} = S\,N\,R\ /400$ and invert Eq. (1) to give the flux level required F_9 to achieve some desired $S\,N\,R_{400}$, we obtain

$$F_9 = 8.5 \left(\frac{R_{30}}{\lambda_{150}} \right)^2 \frac{a_2}{A_{100}} SNR_{400}^2 \ . \quad (2)$$

The much lower *IUE* sensitivity was sufficient to reveal the celebrated discrete absorption components (DACs), but widespread wind clumping by the line-deshadowing instability (LDI) could have lateral sizes of a few Sobolev scale,requiring the much higher $S\,N\,R$ this experiment is designed for.

Published in : Astrophysics and Space Science (2022), vol. 367, n°123
DOI: 10.1007/s10509-022-04142-6
Status : Postprint (Author's version)

The target list compiled for the *Polstar* satellite proposal (Scowen et al. 2022, this volume) was found to exhibit a distribution roughly following 300 $F_9^{-2/3}$ targets brighter than F_9. Applying this relation to any dynamic spectra of the brightest nearby massive stars, we can replace F_9 in Eq. (2) in favor of the desired number of targets N for the survey, resulting in

$$N \cong 70 \left(\frac{\lambda_{150}}{R_{30}}\right)^{4/3} \left(\frac{A_{100}}{a_2}\right)^{2/3} SNR_{400}^{-4/3}. \quad (3)$$

This approximates the distribution of targets over $S\,N\,R$, and shows that many dozens of targets are available at extremely high $S\,N\,R$ for this type of experiment.

Even if the effective area $A100$ falls somewhat below unity over an important part of the spectrum (and the *Polstar* satellite has A_{100} near 0.45 at 150 nm in high resolution), Eq. (3) shows that the dependence of the number of targets on A_{100} is weak enough that 40–50 targets will still be accessible, which is an optimal number given the time available in an experiment able to invest months obtaining several-day continuous monitoring of each target. Thus we conclude that an effective area approaching 50 cm^2 is optimal for this type of study. Assuming a total detection efficiency of order 1%, this points to an aperture at the 50–100 cm level, consistent with a NASA MIDEX mission like *Polstar*.

A larger effective area afforded by a larger aperture would reduce the brightness threshold and allow a wider range of targets of special interest to reach the desired $S\,N\,R$ levels, such as including more O stars with strong enough winds to potentially affect their evolution. But achieving this with larger aperture comes at substantial increase in cost, so a more optimally cost effective strategy for achieving this flexibility in target choice can be accessed by binning the wavelength resolution to the sound-speed scale, $R = 15,000$. It is seen from Eq. (2) that halving the resolution reduces the flux threshold by a factor of 4, while maintaining extremely high $S\,N\,R = 400$ at the sound-speed scale, and $S\,N\,R \sim 300$ at the Sobolev scale. This strategy allows a total of 15 O stars to satisfy the desired threshold with the effective area of *Polstar*, and extends Table 1 to the lower fluxes shown below the indicated line. Observing strategies and target selection can also be modified during a mission in reaction to the discoveries made.

3. Target list

As mentioned, it is especially important to observe clumpy dynamics in the strong winds of O stars, for which massloss corrections can make the greatest difference for the subsequent evolution. Thus strong winds are a priority, but clumpy dynamics in B stars are also important to understand, because this constrains the physics of line-driven winds from a wider perspective, placing the stronger winds into a larger context. Also, continuous spectra with high time and wavelength resolution for B stars supports other spectropolarimetric objectives, such as proposed for *Polstar*, and the same data can be binned in wavelength and time as needed for each individual objective.

Published in : Astrophysics and Space Science (2022), vol. 367, n°123
DOI: 10.1007/s10509-022-04142-6
Status : Postprint (Author's version)

Table 1. *Polstar* targets for structured wind studies

Target	Name	Type	Flux	SNR
HD 122451	β Cen	B1III	600	2200
HD 108248	α Cru	B0.5IV+B1V	600	2200
HD 116058	α Vir	B1III-IV+B2V	530	2000
HD 11123	β Cru	B0.5III+B2V	400	1800
HD 68273	γ Vel	WC8+O7.5III	260	1400
HD 66811	ζ Pup	O4If(n)p	230	1300
HD 37742	ζ Ori	O9.5Iab+B1IV*	200	1200
HD 116658	α Vir	B1III-IV+B2V	200	1200
HD 35468	γ Ori	B2V	190	1200
HD 52089	ϵ CMa	B2II	180	1200
HD 44743	β CMa	B1II-III	160	1100
HD 36486	δ Ori	O9.5II+B1V*	150	1100
HD 149438	τ Sco	B0.2V	130	1000
HD 5394	γ Cas	B0.5IVe	100	900
HD 205021	β Cep	B0.5IIIs	100	900
HD 37043	ι Ori	O9III+B0.8III	100	900
HD 37128	ϵ Ori	B0 Ia	100	900
HD 38771	κ Ori	B0.5 Ia	100	900
HD 34085	β Ori	B8Ia	90	800
HD 127972	η Cen	B1.5Vne	90	800
HD 143018	π Sco	B1V+B2V	75	700
HD 151890	μ^1 Sco	B1.5V+B6.5V	70	700
HD 143275	δ Sco	B0.3IV+B1-3V	70	700
HD 105435	δ Cen	B2Vne	55	600
HD 106490	δ Cru	B2IV	55	600
HD 87901	α Leo	B8IVn	50	600
HD 36861	λ Ori	O8 III((f))	40	550

Published in : Astrophysics and Space Science (2022), vol. 367, n°123
DOI: 10.1007/s10509-022-04142-6
Status : Postprint (Author's version)

HD 120307	ν Cen	B2IV	40	550
HD 136298	δ Lup	B1.5IV	37	500
HD 157246	γ Ara	B1Ib	35	500
HD 205021	β Cep	B1IV	35	500
HD 120324	μ Cen	B2IV-Ve	34	500
HD 147165	σ Sco	B1III+B1V	32	500
HD 11415	ϵ Cas	B3V	31	490
HD 52089	ξ CMa	B1III	30	490
HD 121743	φ Cen	B2IV	30	490
HD 37202	ζ Tau	B2IIIpe	30	490
HD 143118	η Lup	B2IV+A5Vp	30	490
HD 50013	κ CMa	B1.5Ve	29	480
HD 19356	β Per	B8V+K0IV	27	460
HD 125238	ι Lup	B2.5IV	27	460
HD 3360	ζ Cas	B2IV	27	460
HD 10144	α Eri	B6Vpe	27	460
HD 47839	15 Mon	O7.5 V((f))	20	400
HD 10516	φ Per	B2Vep	15	350
HD 24912	ξ Per	O7.5III(n)((f))	13	300
HD 149757	ζ Oph	O9.5V	10	280
HD 38666	μ Col	O9.5 V	10	280
HD 91316	ρ Leo	B1 Iab	10	280
HD 165024	θ Ara	B2 Ib	10	280
HD 64760	J Pup	B0.5 Ib	10	280
HD 53138	O^2 CMa	B3 Ia	10	280

With this in mind, potential targets were considered as part of the *Polstar* proposal, and included 44 targets brighter than the $F9 > 20$ threshold, where F_9 is the UV flux in units of 10^{-9} erg cm^{-2} s^{-1} nm^{-1}. This threshold is chosen to satisfy Eq. (2) even for effective area somewhat below 100 cm^2. An additional 8 targets with sufficient luminosity to support strong winds are also included below the

Published in : Astrophysics and Space Science (2022), vol. 367, n°123
DOI: 10.1007/s10509-022-04142-6
Status : Postprint (Author's version)

line in Table 1, accessible using the flexible strategy described earlier. An asterisk in the spectral type is used to flag when there are additional hot stars in the binary system.

The total list in Table 1 includes 52 targets, providing ample statistical significance for seeking correlations with various types of stellar attributes including rotation rate and binarity, even if only a subset of that full list is ultimately targeted based on lessons learned on the fly. A particularly important subset is near-critical rotators, as their several-day periods allow continuous monitoring over multiple rotation periods to separate periodic from stochastic dynamics.

Polarimetric objectives can also benefit from this very same dataset by using extensive stacking in time and binning in wavelength, as necessary to achieve unprecedented UV polarization precision. For example, for a median star from the list like γ Cas, stacking over 2-hour chunks to allow temporal resolution of longer-lived structures on the scale of the wind flow time, and binning to $R = 30$ to focus on continuum polarization, would allow a *SNR* of some 1×10^5 per resolution element for an instrument with effective area approaching 100 cm^2. Even with somewhat lower effective area, as for *Polstar's* high-resolution channel, a polarization precision at the level of 3×10^{-4} is supported, with sufficiently many resolution elements to remove foreground polarization from the interstellar medium (Andersson et al. 2022, this volume). Separation from background polarization is also assisted by the time-varying nature of intrinsic polarization stemming from stochastic wind clumping.

Such polarization information brings out processes that break the spherical symmetry, either over wind flow times or in global steady state, while the dynamic spectra reveal evolving processes on much smaller spatial and temporal scales. Note also that any spectropolarimeter that determines all four Stokes parameters, I , Q, U, and V , in all its observations, such as *Polstar*, will obtain this polarimetric information automatically, as it compiles spectral information in the time domain.

All told, high-resolution UV spectropolarimetry allows combining dynamic spectra with linear polarization variations to track clumpy structures in the time domain right down to the Sobolev scale, as well as larger CIR velocity plateaus, as they accelerate through the winds of 40–50 galactic massive stars, to understand clumping and structure formation, and their impact on wind mass-loss rate determinations. It can also detect global nonspherical structures with very small latitudinal differences in optical depth $\cong 0.01$, due to rotation, orbit, or magnetism, as well as rotationally modulated polarization from large-scale longitudinal structures such as CIRs and mass-transfer streams.

4. Diagnostics of small-scale clumps

Due to the variability of spectral lines, as well as the presence of linear polarization, astronomers have known for decades that stellar winds are nonspherical and nonsteady (e.g. Puls et al. 2008), Motivated by hydrodynamic simulations (e.g., Feldmeier et al. 1997; Sundqvist and Owocki 2013) including the line-deshadowing instability (LDI) (Owocki et al. 1988), extreme density variations are expected to lead to large root-mean-square density ratios, $D = \sqrt{< \rho^2 >} / < \rho >$, which is the inverse

Published in : Astrophysics and Space Science (2022), vol. 367, n°123
DOI: 10.1007/s10509-022-04142-6
Status : Postprint (Author's version)

square root of the "volume filling factor" *f* when the interclump medium is regarded as void (an unnecessary assumption not made here).

For continuum opacity that is independent of density, such as free-electron opacity κ_{es} , the mean opacity is the same for smooth or clumpy winds of the same mass flux. But opacity (in the sense of cross section per gram) that scales with density (such as for recombination lines like Hα) is enhanced by the clumping factor *D*, subject to a fixed observed collisionally created "density squared" emission flux. When such emission flux is held fixed, as observationally required, *D* gives the ratio of smooth-wind mass-loss rate to actual mass-loss rate. Thus *D* is a well-defined one-parameter fit to the complex details of the clumping distribution, and we wish to complement optical fluxes with UV line shapes and polarization to infer *D* and disentangle its various local and global contributors.

Relatively large *D* values in the 2–10 range, possibly due to extensive micro-clumping (clumps on size scales smaller than a continuum mean-free-path) are often reported in hotstar winds. This implies a reduction of order ~2–3 (i.e., $\sqrt{D}$) in older estimates of mass-loss rates derived from collisional emission processes in the optical and radio regimes (Mokiem et al. 2007).

This important *D* parameter is difficult to accurately quantify and may often be dominated by small dynamical features. Still, the Doppler shifts of these features evolve in the time domain in a way that can be tracked by continuous high-resolution UV spectrometry. Such continuous tracking takes advantage of the resonance line opacity that is liberally sprinkled throughout the UV, covering a wide range from strong to weak lines, allowing access to wind regions both close to and far from the star, and over a range of wind massloss rates.

One challenge with metal resonance lines is that the abundances and degree of ionization can be poorly known. In the FUV, the degree of ionization can be simplified because the P V λλ1118, 1128 stage is expected to dominate in certain O stars, so its absorption column should in principle provide an accurate estimate of the mass-loss rate. To this end, Fullerton et al. (2006) selected a large sample of Ostars, which also had mass-loss rate estimates from Hα and radio, and found that using a simple "filling factor" clumping model to fit the observed line profiles led to large clumping factors up to *D* ~ 10 (e.g. Bouret et al. 2003).

But UV resonance lines are more complicated than a simple filling factor approach can accommodate, because the Sobolev optical depth in such lines depends not only on density, but also on velocity gradient, via the combination $\rho(dv/dr)^{-1}$. Since the local acceleration, and hence *dv/dr*, depends self-consistently on density, the Sobolev optical depth scales more steeply than linear in density. For example, if we neglect time dependent terms in the force equation (a rough approximation), and also neglect any feedback between density and line opacities (also a crude simplification), then at given velocity *v* and radius *r*, the standard treatment using the CAK α parameter gives

$$\frac{dv}{dr} \propto \rho^{\alpha} \left(\frac{dv}{dr} \right)^{-\alpha} . \quad (4)$$

Published in : Astrophysics and Space Science (2022), vol. 367, n°123
DOI: 10.1007/s10509-022-04142-6
Status : Postprint (Author's version)

With $\alpha \cong 2/3$, we then have $dv/dr \cong \rho^{-2}$, which implies the Sobolev optical depth in the UV resonance line in question obeys $\tau \propto \rho(dv/r)^{-1} \propto \rho^3$.

This represents quite a steep dependence of optical depth on density variations, allowing spatial regions of low density to yield open holes in velocity space where there is low line optical depth, an effect termed "vorosity" (Owocki and Sundqvist 2018) in analogy with the "porosity" concept for spatial holes in continuum opacity. Hence optically thick clumping can reduce the degree of absorption in a P Cygni trough (Sundqvist et al. 2018), because the vorosity allows a window through the normally optically thick line, to a degree we wish to better characterize. Methods restricted to a purely *spatial* "filling factor" would overlook this vorosity effect, and thus the observed desaturation of P Cygni-type absorption could lead to unnecessarily excessive reductions in the inferred mass-loss rate.

4.1 OPTICALLY THICK CLUMPING ("MACRO"-CLUMPING)

Some analysis of optically thick clumping effects in resonance lines has already been undertaken, taking into account more than just the "filling factor" D, but also the distribution, size, and clump geometry. The conventional description of macro-clumping is based on a clump size, l, and an average spacing of a statistical clump distribution, L, with porosity length $h = L^3/l^2$ (Owocki and Sundqvist 2018). This porosity length h represents the key parameter defining a clumped medium, as it corresponds to the photon mean free path in a medium consisting of optically thick clumps.

Oskinova et al. (2007) employed an "effective opacity" concept in the formal integral for line profile modeling of the well-studied O supergiant ζ Pup. Figure 2 shows that the most pronounced effect involves strong resonance lines, such as the resonance doublet P V λλ1118, 1128 which can be reproduced by this macro-clumping approach – without the need for extremely low $\dot{M}$ – resulting from an effective opacity reduction when clumps become optically thick.

Given that *Hα* remains optically thin for O-type stars, its line profile shape is not affected by porosity and it can be reproduced simultaneously with P V λλ1118, 1128. This enabled a solution to the P V λλ1118, 1128 problem (see e.g. Šurlan et al. 2013, Sundqvist and Puls 2018), but details of the clumping (such as vorosity effects) alter the quantitative corrections to the mass-loss rate, and a careful investigation of clumped structure is needed.

P Cygni-type absorption has the advantage of sampling only the narrow column to the star itself, suffering significantly less spatial averaging than emission-based diagnostics and offering higher fidelity for mapping time-dependent Doppler shifts. Thus we intend to use UV line shapes and variability to provide more powerful constraints on the *D* parameter, to facilitate mass-loss rate corrections and better understand the driving mechanics, in ways described next.

Published in : Astrophysics and Space Science (2022), vol. 367, n°123
DOI: 10.1007/s10509-022-04142-6
Status : Postprint (Author's version)

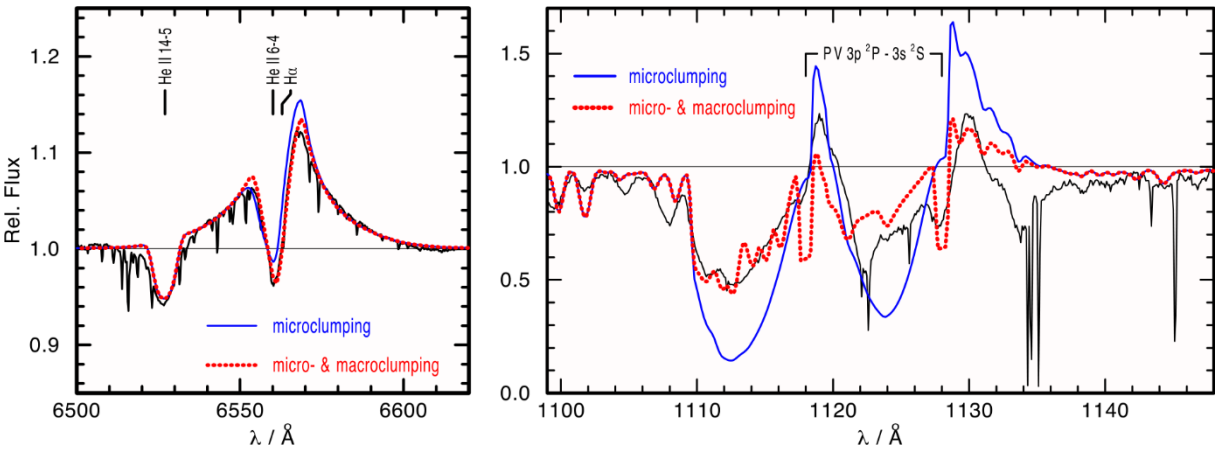

Fig. 2 Porosity as the likely solution for the PV problem. The Hα line on the left-hand side is hardly affected by macro-clumping, while the P V λλ1118, 1128 UV line on the right is strongly affected. Adapted from Oskinova et al. (2007)

4.2 P CYGNI EQUIVALENT WIDTH

The most basic way that clumpy wind structure affects P Cygni-type line profile diagnostics is in its impact on line equivalent width (EW), in the blueward absorption trough and the redward emission hump, as well as the total of both. Clumping affects these because even for purely scattering lines, the total EWis affected by the fraction of line photons reflected back to the star, relative to the EWs in the absorption and emission features. Vorosity effects reduce all these EWs in ways that can masquerade as a lower wind column depth, as mentioned above, and an approach for correcting this problem is suggested here.

For saturated absorption with no turbulent clumping, the absorbed (negative)EW, in velocity units, would be the wind terminal speed. The full EW on the blue side of the line would be half that, owing to the fore/aft symmetry of scattering from the forward (blueshifted) hemisphere. That latter component would also give the (positive) equivalent width on the red side, except the fraction of the scattered emission that is occulted by the star must be estimated and subtracted.

Figure 3 shows that the occultation encountered for a velocity law of the form $v(r) \propto (1 - R/r)^{\beta}$ generally reduces the EW in the red bump of a strong line from the abovementioned 1/2 to about 1/3, again in terminal speed units. This also implies that the ratio of the red-bump EW to the total EW across the entire line is about $(1/3)/(1/2 + 1/3 - 1) \cong -2$ for a strong line in a smooth spherical wind. This is roughly consistent with the blue curve in Fig. 2, which is only weakly affected by microclumping.

In contrast, the observed profile in Fig. 2 exhibits a much weaker red-bump EW than the smooth-wind prediction, relative to its total line integrated EW (focusing on the red line from the doublet, since it is less affected by the doublet pair). This indicates that the role of wind macroclumping (that is, clumping on scales larger than the Sobolev length, so the clumping induces large variations in the line optical depth along different lines of sight at a given observed wavelength in the line) is to strongly increase photon destruction within the linewidth, resulting in a larger (negative) total EW.

Published in : Astrophysics and Space Science (2022), vol. 367, n°123
DOI: 10.1007/s10509-022-04142-6
Status : Postprint (Author's version)

This may be due to increased return of photons to the stellar photosphere by virtue of how the locally steep velocity gradients expected in lower density regions favor radial escape from the optically thick resonance zones of strong lines, beaming a larger fraction of their scattered line photons back to the photosphere, where they can be absorbed by continuum processes. Modeling these effects on line photon escape, in the context of a detailed clumping model, can constrain the local velocity gradients associated with that model.

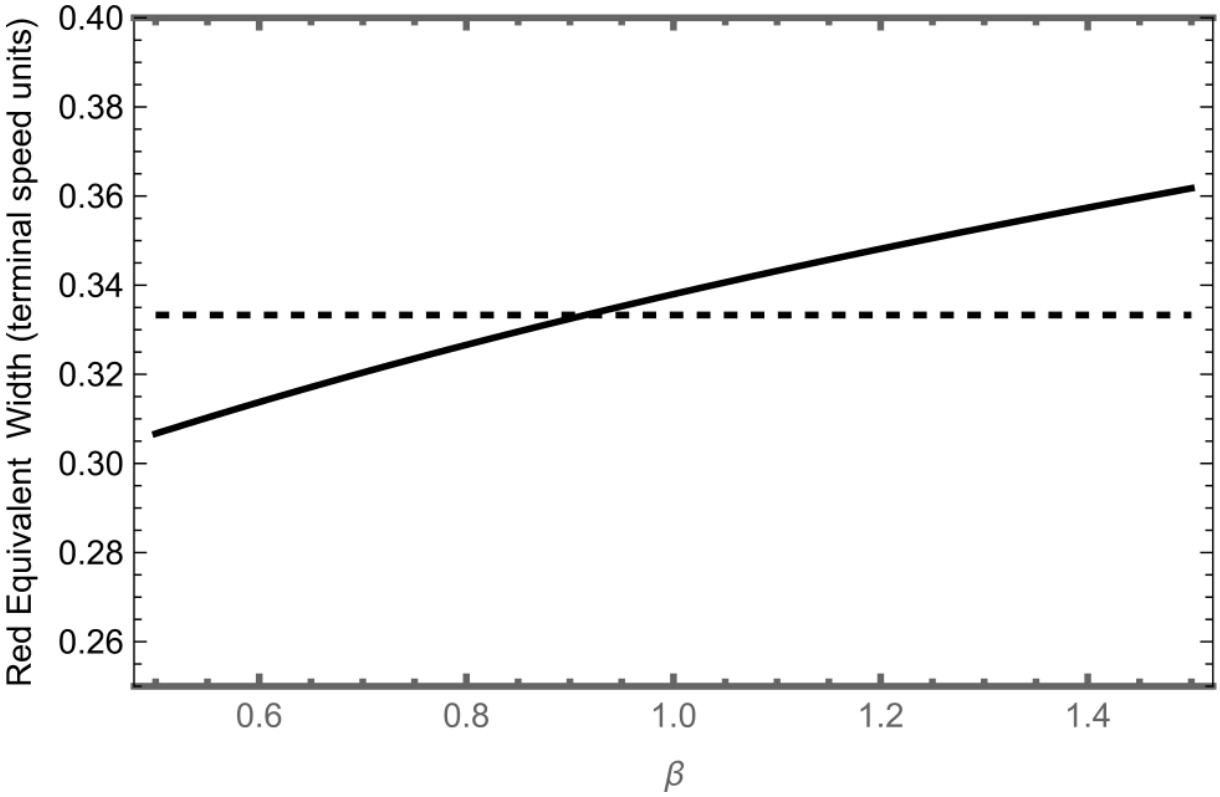

Fig. 3 Equivalent width, in units of fraction of wind terminal speed, of the red bump of a hypersonic P Cygni profile under the assumption of pure scattering in an extremely optically thick line, in the absence of clumping and for the given β of the velocity law. Stellar occultation is the source of the (weak) dependence on β. Indicated for reference is the approximate smooth-wind saturated-line red bump equivalent width of 1/3, similar to the redmost bump in the blue curve of Fig. 2

4.3 BEYOND FILLING-FACTOR APPROACHES

A somewhat more sophisticated type of density variance model would be to assume the density inhomogeneities induce a log-normal distribution over density ρ. Thus we might assume

$$\frac{dp}{d\ln\rho} = \frac{e^{-(\ln(\rho/\bar{\rho})/\sigma)^2}}{\sqrt{\pi}\sigma} \tag{5}$$

describes the (normalized) probability distribution of the densities, relative to the local mean density $\bar{\rho}$., that photons encounter as they traverse the wind. Here σ characterizes the logarithmic density variance, and when taken as constant, it corresponds to the clumping factor *D* via

Published in : Astrophysics and Space Science (2022), vol. 367, n°123
DOI: 10.1007/s10509-022-04142-6
Status : Postprint (Author's version)

$$D = \frac{\sqrt{<\rho^2>}}{<\rho>} = e^{\sigma^2/4}. \quad (6)$$

The effect of the inhomogeneity on wind absorption for strong lines that would normally be saturated if $\sigma \to 0$ is then approximated by truncating the integral for $< e^{-\tau} >$ for resonance line (Sobolev) optical depth τ above unity, resulting in the complementary error function expression

$$< e^{-\tau} > \cong \frac{1}{2}\mathrm{erfc}\left(\frac{\ln(\dot{M}/\dot{M}_1)}{3\sigma}\right). \quad (7)$$

Here $\dot{M}_1$ is the theoretical smooth spherical mass-loss rate necessary to produce . $\tau = 1$, and $\dot{M}$ is the actual (clumpy) mass-loss rate. Note the factor 3 that appears in the denominator is from the earlier derived $\alpha = 2/3$ result $\tau \propto \rho^3$, so this important factor stems from the vorosity effect and implies that vorosity acts to effectively triple the logarithmic variance in the Sobolev optical depth as compared to the density. That effect significantly desaturates line absorption, requiring a much smaller reduction in mass-loss rate to fit observed line profiles.

Since our approach is to imagine that observed collisionally induced emission is to be held constant as we test different amounts of clumping, we can define a smooth spherical mass-loss rate $\dot{M}_s$ via

$$\dot{M}_s = D\dot{M} = \dot{M}e^{\sigma^2/4}. \quad (8)$$

Then note that since $\dot{M}_s$ is fixed by observations, while $\dot{M}_1$ is known from the strength of the line in question, we have

$$< e^{-\tau} > \cong \frac{1}{2}\mathrm{erfc}\left(\frac{\ln(\dot{M}_s/\dot{M}_1)}{3\sigma} - \frac{\sigma}{12}\right). \quad (9)$$

Equation (9) quantifies in this approximation the desaturation of the UV P Cygni-type absorption, given the logarithmic density variance σ , allowing *D* to be inferred. That leads to the correction for the actual $\dot{M}$, relative to the smooth $\dot{M}_s$ constrained by observed optical or radio emission diagnostics. Since σ will generally be order unity, and Eq. (9) applies only to strong lines ($\dot{M}_s > \dot{M}_1$), the first term in the argument will usually dominate. This term stems from the holes in the absorption being created by the clumping, whereas the second term gives a small correction for having to reduce the true $\dot{M}$ relative to the observed $\dot{M}_s$ constraint. The key point is, this necessary reduction is much less than it would be if the vorosity effect, leading to the 3 in Eq. (7), were not included.

Published in : Astrophysics and Space Science (2022), vol. 367, n°123
DOI: 10.1007/s10509-022-04142-6
Status : Postprint (Author's version)

4.4 THE ORIGIN OF WIND CLUMPING

In the standard view of structure formation via the LDI, clumping would be expected to develop only after the instability has had sufficient opportunity to amplify small initial perturbations. For typical O-star winds, this should have occurred by half the terminal wind velocity, so about half a stellar radius from the surface, but not sooner.

Various observational indications, including the existence of linear polarization (e.g. Davies et al. 2005) and radial dependent Stokes I diagnostics (Puls et al. 2006) indicate that some clumping already exists at very low velocities, and likely arises inside the stellar photosphere. Cantiello et al. (2009) suggested that waves produced by the subsurface convection zone could lead to velocity fluctuations, and possibly density fluctuations, and could thus be the root cause for the wind clumping seen close to the stellar surface.

Assuming the horizontal extent of the clumps to be comparable to the vertical extent, and both scaled to the subphotospheric pressure scale height H_p, one may estimate the number of convective cells by dividing the stellar surface area by the surface area of a convective cell, thus scaling as $(R/HP)^2$. For main-sequence O stars in the canonical mass range 20–60 $M_\odot$, pressure scale heights are within the range $\sim 0.05-0.2R_\odot$, corresponding to total clump numbers roughly in the range $6\times10^3-6\times10^4$. These estimates could be tested through linear polarizationmonitoring, probing wind clumping close to the wind base.

In an investigation of linear polarization variability in WR stars, Robert et al. (1989) revealed an anti-correlation between the terminal velocity and the observed scatter in linear polarization. They interpreted this in terms of blobs growing or surviving more effectively in slower winds. Davies et al. (2005) found this trend to continue into the lower temperature regime of the luminous blue variables (LBVs), whose winds are even slower, and they found the polarization position angles of LBVs to vary irregularly with time, which was attributed to wind inhomogeneity. Given the short timescale of this variability, Davies et al. (2005) argued that LBV winds consist of order thousands of clumps near the surface.

Correlations between polarization variability and wind dynamics, including wind terminal speed, across a wide class of hot stars, offers additional and complementary information about the nature of wind driving. However, this requires previously unavailable high S/N at the level of 2×10^{-4}, to derive the numbers of wind clumps and their sizes from polarimetry. These are attainable goals with the proposed *Polstar* mission when binned to $R\cong30$, providing ample wavelength resolution for separating foreground sources.

5 Diagnostics of large-scale structure

Inferences of wind mass-loss rate can also be affected by large-scale structures that are either steady, or quasi-steady, over many wind flow times. In single stars, these could be due to coherences in nonradial pulsations, gravity waves or other types of buoyant convection that perturb the stellar

Published in : Astrophysics and Space Science (2022), vol. 367, n°123
DOI: 10.1007/s10509-022-04142-6
Status : Postprint (Author's version)

surface, rotation, or long-lived magnetic fields. Each of these have their own spectroscopic and polarimetric signatures that need to be understood to form a more complete picture of how massive stars interface with their surroundings.

5.1 MAGNETICALLY CONFINED WINDS

Magnetic fields can influence hot-star winds significantly, often leading to large-scale structures. In theory, their overall influence on the wind dynamics can be characterized by a single magnetic confinement parameter,

$$\eta_* \equiv \frac{B_{eq}^2 R_*^2}{\dot{M} v_\infty} \quad (10)$$

which characterizes the ratio between magnetic field energy density and kinetic energy density of the wind, as defined in ud-Doula and Owocki (2002). The effects at large η_* are considered in detail in a companion paper (Shultz et al. 2022, this volume), but since such magnetic influences are also relevant to clumping and wind asymmetry that affects mass-loss rate diagnostics, and can appear even at low values of η_*, we include a short description here.

Extensive magnetohydrodynamic (MHD) simulations show that, in general, for the stellar models with weak magnetic confinement, $\eta_* < 1$ field lines are stretched into radial configuration by strong outflow very quickly on a dynamical timescale. However, even for magnetic confinement as weak as $\eta_* \sim 1/10$ the field can have enough influence to enhance density by diverting the wind material from higher latitudes towards the magnetic equator.

On the other hand, for stronger confinement, $\eta_* > 1$, the magnetic field remains closed over a limited range of latitude and height about the equatorial surface, but eventually is opened into a nearly radial configuration at large radii. Within closed loops, the flow is channeled toward loop tops into shock collisions where the material cools and becomes dense. The stagnated material is then pulled by gravity back onto the star in quite complex and variable inflow patterns. Within open field flow, the equatorial channeling leads to oblique shocks that eventually lead to a thin, dense, slowly outflowing "disk" at the magnetic equator. This is in concert with the "magnetically confined wind shock" model first forwarded by Babel and Montmerle (1997). Such large-scale wind structures are inferred most directly from time variability in the blueshifted absorption troughs of UV P Cygni profiles.

More recent MHD modeling shows that the wind structure and wind clumping properties change strongly with increasing wind-magnetic confinement. In particular, in strongly magnetically confined flows, the LDI leads to largescale, shellular sheets ('pancakes') that are quite distinct from the spatially separate, small-scale clumps in nonmagnetic hot-star winds (Driessen et al. 2021).

Published in : Astrophysics and Space Science (2022), vol. 367, n°123
DOI: 10.1007/s10509-022-04142-6
Status : Postprint (Author's version)

5.2 DISCRETE ABSORPTION COMPONENTS (DACS)

Time-resolved high-resolution FUV spectroscopic observations obtained with the International Ultraviolet Explorer (IUE) showed that DACs start out as broad, shallow absorption features at low velocity, narrowing and deepening (in some cases saturating) as they migrate to higher velocities over characteristic timescales on the order of days (e.g. Prinja et al. 1987). Furthermore, they are found to occur nearly ubiquitously among O stars (Howarth and Prinja 1989)], and since they can saturate the absorption over a significant range of velocities, they must cover a large radial extent within the stellar wind. Clearly these are significant features with an important role to play in line driven winds, yet their cause is still mysterious.

Line variability is seen on multiple scales, so one important question relating to DACs is how they connect to other types of structure, both in the photosphere and the wind. Determining whether UV spectral variability is due to material originating near or at the surface of the star which then propagates outward, or if it originates well out in the wind and is then amplified by the driving forces, is an important question that can be addressed with dynamical spectra of the type planned with *Polstar*. Relevant questions include, how does large-scale wind structure originate, what types of photospheric irregularities could be involved in producing DACs, and what fraction of observed wind X-rays are formed in shocks associated with them.

These questions are complicated by the fact that there is no way to directly determine the location in the wind where an absorption feature at a specific velocity originates. For example, a low velocity feature could lie near the stellar surface and still be in its initial acceleration, or it could be decelerated farther out in the wind by some combination of shocks, radiative cooling, and gravity. Dynamical tracking such features in real time can help resolve this ambiguity in UV resonance lines.

Another strategy for resolving this ambiguity is to consider excited-state lines. An excited-state wind line (ESWL) arises from an allowed transition whose lower level is the upper level of a resonance transition (typically below 900 A, so impossible to observe through interstellar hydrogen clouds). They frequently appear as wind lines in O stars with strong mass fluxes. One of the most commonly observed ESWLs is N IVλ1718 Å, whose lower level is the upper level of the N IVλ765 Å resonance line. Because a strong EUV radiation field is required to populate an ESWL, these lines can only exist close to the star (and this gives them their distinctive shape). Similarly, a feature which appears at low velocity in an ESWL must also originate close to the stellar surface.

Unfortunately, this same property means that ESWLs weaken quickly at large distances from the star and, as a result, cannot be tracked to high velocities. Hence, resonance and excited-state lines complement each other. If an excess or reduced absorption feature is seen at low velocity in an ESWL, then joins a high-velocity feature in a resonance line (whose low-velocity portion may be too saturated to notice), this provides evidence that the excess or deficiency of the absorbing material originated close to the stellar surface, and later propagated outward into the wind.

This motivates the powerful diagnostic of splicing together the temporal behaviour seen in the Si IVλλ1400 Å resonance-line doublet and the N IVλ 1718 Å excited-state singlet (Fig. 4). Such dynamic spectra involve images of time ordered spectra normalized by the mean spectrum of the series. The

Published in : Astrophysics and Space Science (2022), vol. 367, n°123
DOI: 10.1007/s10509-022-04142-6
Status : Postprint (Author's version)

properties of coherent structure seen in the full comparison between these lines will allow us to (i) test whether every absorption feature observed at high velocity connects to a feature at low/zero velocity, or if some features develop gradually within the wind (as expected with the LDI), (ii) establish connections between these wind features and perturbations of the stellar surface, (iii) detect "banana" shaped examples of DACs, which are the accepted signatures of CIRs (a point returned to below), and (iv) compare the relative number of large features that cover a significant solid angle with a potential hierarchy of smaller features.

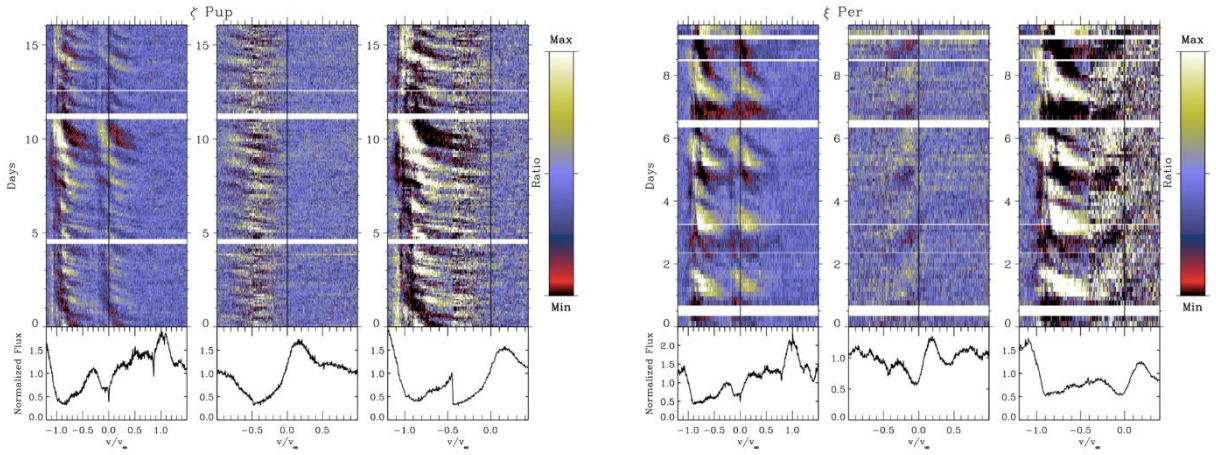

Fig. 4 Dynamic spectra as deviations from the mean profiles shown at bottom, taken from the IUE MEGA project for ζ Pup and ξ Per. Strong (left) and weak (center) lines are spliced together (right) to show the continuous acceleration of the DAC features (Massa and Prinja 2015)

In addition to the question of where the features originate, is when do they represent gas that is advecting with the wind, and when are they velocity features that the gas moves through like a spiral density wave. The former type of feature would move through the line profile in a characteristic wind flow time (v/r), whereas the latter would lag significantly because it represents constantly changing material. DACs are generally considered to accelerate through the line profile over timescales slower than the wind flow time, suggesting the latter scenario, but (Hamann et al. 2001) finds evidence that some UV absorption features in the wind of ζ Pup, possibly separate from DACs, accelerate similarly to advecting structures. Current datasets are too sparse to clearly distinguish these possibilities, or correlate them with feature size and location in the wind, so significant accumulation of UV dynamical spectra in many types of hot stars is needed.

Observations in other wavebands can also assist our understanding of the wind structure, with several observations pointing to a single origin for several forms of variability. For example, (Kaper et al. 1997) detected variability in the Hα profiles of several O stars, on timescales consistent with those characterizing DAC variability observed contemporaneously in the UV. This Hα variability was found to occur only at low velocities, and given that this diagnostic is sensitive only to the densest wind material located near the stellar surface, this strengthens the hypothesis that the low-velocity absorption seen in the UV also originates from that region of the wind.

Moreover, variations of the X-ray broadband flux over timescales compatible with rotation have also been detected for a handful of OB stars (e.g. ξ Per: Massa et al. 2019; ζ Pup: Nichols et al. 2021; ζ Oph:

Published in : Astrophysics and Space Science (2022), vol. 367, n°123
DOI: 10.1007/s10509-022-04142-6
Status : Postprint (Author's version)

Oskinova et al. 2001; and λ Cep: Rauw et al. 2015). These have all been speculated to be associated with DACs and possibly CIRs (see below), but confirmation awaits better constraints from high-resolution, high-sensitivity observations, potentially supplemented with polarization, all of which would be available from UV spectropolarimeters like *Polstar*. Since optical emission represents primarily the high densities in the lower wind, and X-rays represent only the hot shocked gas, UV resonance lines provide the best coverage over the full wind, especially in the context of continuous time coverage. This offers our best chance to unite these disparate lines of evidence into a cogent description of the causes of DACs, and their implications for overall wind-driving mechanics.

5.3 COROTATING INTERACTION REGIONS

As mentioned above, one of the leading hypotheses to explain DACs involves large-scale spiral structures extending through most of the radial extent of the wind, termed CIRs Mullan (1986) in analogy with similar features in the solar wind. In this model, wind features are anchored in long-lived photospheric inhomogeneities in either brightness, motion, density, magnetism, or some combination thereof. Stellar rotation then maps these long-lived inhomogeneities into spiral streaklines, which cross the line of sight to the observer at points of different phase along the streakline as the star rotates. This reveals different wind conditions as a function of the changing relative angle to the persistent inhomogeneity on the stellar disk. The changing Doppler shift where the feature crosses the line of sight thus propagates through the UV absorption line, which could be the primary cause of DACs (Cranmer and Owocki 1996).

One way to achieve this quasi-periodic footpoint modulation is to adopt *ad hoc* bright spots on the stellar surface (as dark "sunspots" were found to fail to match observations, Cranmer and Owocki 1996). These bright spots enhance the local radiatively driven mass flux, inducing a slight overdensity within the CIRs, but the primary source of the enhanced absorption in the resulting DACs stems from the velocity plateau (or "kink") that arises when rarefied, accelerated material plows into this denser, slower material. More recent hydrodynamical simulations including the effects of spots whose properties are constrained by modern space-based broadband optical photometry (Ramiaramanantsoa et al. 2014) reproduce similar results, and coupling the obtained wind structure with an appropriate radiative transfer scheme yields synthetic spectra with DACs whose qualitative and quantitative properties are compatible with those of observed DACs. Such simulation efforts were also extended to 3D (Dessart 2004).

The combination of high spectral resolution with high SNR, such as with *Polstar*, should significantly advance our understanding of the structures responsible for DACs. The IUE MEGA campaign well characterized DACs in the time domain for only a few targets, and at a SNR that could only detect the largest features. Whether these large features are separate from the small-scale clumping, and its associated vorosity needed to desaturate P Cygni absorption profiles, or part of a continuous hierarchy of structures, can only be answered via a more dedicated study at higher SNR.

What is more, the advantage that absorption focuses on a narrow column to the star comes with the disadvantage that it cannot directly connect that column to the global geometry. Similarly, the ability of Doppler shifts to connect to high spectral resolution comes with the disadvantage that the

Published in : Astrophysics and Space Science (2022), vol. 367, n°123
DOI: 10.1007/s10509-022-04142-6
Status : Postprint (Author's version)

information is in the velocity domain rather than the spatial domain. Hence the physical structures remain ambiguous when all available information relates to their velocity projected against the face of the star. Hence the polarimetric capability of *Polstar* will also be valuable.

The potential for spectroscopic complexity is exhibited in Fig. 5, where shown is the resonance zones in a CIR-type model structure. Dynamic spectra include a wealth of information from the time domain involving structure along the path to the stellar disk, but polarization is most sensitive to right-angle scattering, so provides complementary information from the wind patterns outside that column.

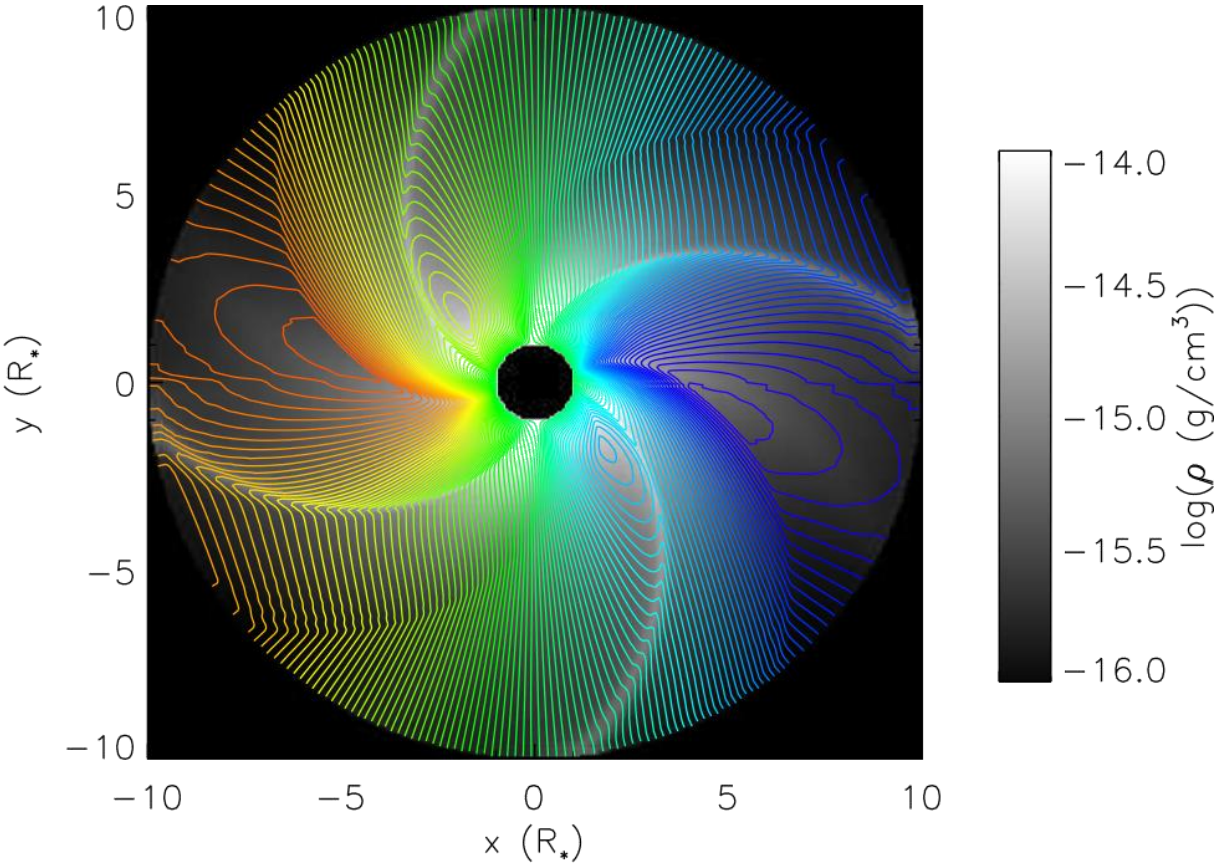

Fig. 5 Adapted from David-Uraz et al. (2017): 2D equatorial slice of a hydrodynamic simulation of a wind with CIRs created by four equally spaced bright spots. The greyscale background represents density, and color-coded line-of-sight isovelocity contours are overlaid for an observer along the positive x-axis (blue corresponds to high-velocity blue-shifted material, and red to high-velocity red-shifted material). A 50 km s^{-1} resolution is shown, illustrating that the ~10 km s^{-1} resolution achievable with *Polstar* will spatially sample the complex structure of the wind material very effectively. This will continue to be true when the data is binned to 20 km s^{-1} resolution to obtain the high SNR desired in this experiment. The figure demonstrates that when large-scale structure is present, spatial resolution cannot be simply interpreted from the Doppler shifts in the line profile; additional geometric information from continuum polarization will be necessary to resolve ambiguities in the global structure

Polarization information from Ch1 is automatically obtained along with the *Polstar* dynamic spectra, and binning to low resolution increases the sensitivity dramatically. The foreground polarization from dust in the interstellar medium will be separated from the intrinsic signal in ways informed by

Published in : Astrophysics and Space Science (2022), vol. 367, n°123
DOI: 10.1007/s10509-022-04142-6
Status : Postprint (Author's version)

the analysis of Andersson et al. (2022, this volume). This involves wavelength-dependent signatures that only require on the order of 30 points per spectrum, rather than the 30,000 available in the dynamic spectra, so binning by a factor of 1000 will be used to raise the *SNR*. Since features that move rapidly through the spectral resolution need not be tracked in the polarization observations, temporal stacking is also possible, up to dynamical times of a few hours, and together this stacking and binning allows the *SNR* to be raised from the > 400 value shown in Table 1 to > 10, 000, suitable for the required 3×10^{-4} polarization sensitivity target.

The DACs themselves can be well characterized at IUE SNR levels, but their impact on the inferred mass-loss rates is only significant if they represent the large-scale limit of a hierarchy of smaller structures that IUE did not have the SNR to detect.

An important clue to the nature of DACs stems from their persistence timescales. Although they often repeat in the dynamic spectra of OB stars (e.g. Kaper et al. 1996), they are not strictly periodic. Nevertheless, they are characterized by a timescale that may often be related to the rotation period of a star (Prinja 1988). Anchoring the modulation to rotation prompted the hypothesis that CIRs could be a consequence of large-scale surface magnetic fields, though such fields have since been detected on only a small subset of massive stars (Grunhut et al. 2017), as discussed above.

Using high-quality optical spectropolarimetric data, David- Uraz et al. (2014) have placed stringent upper limits on the magnetic field strengths of a sample of 13 well-studied OB stars with extensive FUV time-resolved spectra. They conclusively demonstrate that large-scale fields could not exert sufficient dynamic influence on the wind to form CIRs. An alternative explanation involves non-radial pulsations (NRPs), but reconciling their typical periods with the DAC recurrence timescales requires complex mode superpositions (de Jong et al. 1999). Therefore, the prevailing hypothesis regarding the origin of putative CIRs involves the presence of spots on the stellar surface, and this hypothesis begs further testing.

5.4 SURFACE SPOTS

Spots of enhanced brightness on hot-star surfaces is an important possibility for our understanding of the structure of massive stars, which goes beyond presenting a promising cause of CIR structures. UV photometry supports their study, and *Polstar* might provide sufficient relative photometric stability (over the several-day observational timescales involved) to weigh in on the topic. This could inform the currently unsettled state of theoretical explanations for the orgin of bright spots.

Unlike lower-mass Ap/Bp stars and chemically peculiar intermediate mass stars (such as Am stars and HgMn stars), early-type OB stars are not expected to have chemical abundance spots, as they would be continuously stripped by the wind (e.g. Michaud et al. 1987). One possible mechanism for producing bright spots involves small-scale magnetic fields, whereby locally enhanced magnetic pores (perhaps from convective motions in the subsurface convection zone due to the iron opacity peak (FeCZ; Cantiello et al. 2009; Schultz et al. 2020), could reduce the gas pressure involved in the lateral force balance, creating lower opacity that allows stellar continuum photons to escape from deeper, hotter, brighter regions (Cantiello and Braithwaite 2011).

Published in : Astrophysics and Space Science (2022), vol. 367, n°123
DOI: 10.1007/s10509-022-04142-6
Status : Postprint (Author's version)

Growing observational evidence suggests this may occur in a variety of massive stars not observed to have globally strong fields (e.g., Balona 2019; Momany et al. 2020), and weak structured fields have now been detected on several Atype stars (e.g. Petit et al. 2017). There have also been further theoretical advances suggesting that stars with radiative envelopes can either have large-scale fields strong enough to inhibit convection in the FeCZ, or weak, disorganized fields generated by that convection (Jermyn and Cantiello 2020), leading to a bimodal distribution of field strengths and thus explaining the so-called 'magnetic desert' (Aurière et al. 2007).

An alternative explanation regarding the origins of spots and CIRs is that they are generated directly due to waves and oscillations propagating to the stellar surface, locally affecting UV brightness and gas launching at the wind base. While non-radial pulsations (NRPs) have traditionally been invoked in this context (e.g. Fullerton et al. 1996), the mode superpositions required to reproduce the observed timescales pose difficulties (de Jong et al. 1999). Instead, the more recent discovery of ubiquitous stochastic lowfrequency variability in OB stars, associated with internal gravity waves that either propagate from the convective core (Bowman et al. 2020), or are the result of turbulent motions generated in the FeCZ (Lecoanet et al. 2019), might also be able to explain the characteristic DAC timescales.

In either case, the weakness of the observed photometric variations place constraints on the size and brightness of spots that could seed wind features large enough to explain DACs, as investigated in David-Uraz et al. (2017). At present, bright spots have been detected on at least two archetypal massive stars: ξ Per (Ramiaramanantsoa et al. 2014) and ζ Pup (Ramiaramanantsoa et al. 2018). These initial studies suggest that the spots are large (angular radius greater than ∼10°) and relatively persistent (lasting roughly tens of rotational cycles), and lead to fairly faint variability (about 10 mmag in the optical – only detectable with space-based facilities). Further hydrodynamical simulations carried out by David-Uraz et al. (2017) showed that the spot properties inferred from the light curve of ξ Per could also lead to CIRs that quantitatively reproduce the DACs observed for this star.

Polarimetric observations on rotational timescales can also contribute to the study of spots. A bright spot at the level of 10 millimags that is located away from the center of the stellar face would break the polarization cancellation otherwise present in smooth spherical symmetry. The polarization signature of bright spots would be detectable and quantifiable at sensitivities better than 10^{-3}, as targeted by the *Polstar* mission.

The resulting polarization would be identified by its characteristic wavelength dependence, stemming from the wave-length dependence of the brightness increase (which would induce a greater contrast in the FUV closer to the spectral peak). The polarization position angle would also evolve as the spot moves in real time, and the degree of polarization would modulate on the rotational period as well, making it easier to separate from ISM polarization contributions (more details about removing the ISM polarization are given in Andersson et al. 2022, this volume). Polarizationmeasurements tracked in real time would thus provide unique constraints on the location and size of the dominant spots, informing their origins and their relationship to simultaneous wind features.

Published in : Astrophysics and Space Science (2022), vol. 367, n°123
DOI: 10.1007/s10509-022-04142-6
Status : Postprint (Author's version)

6. Hydrodynamicmodeling

Advances in radiation hydrodynamics allows timely theoretical support for *Polstar* objectives. Recent models of the line-driven instability (LDI) using 2D hydrodynamics driven by 1D radiative transfer, simplified to allow dynamical resolution of the resulting clumping, gives the density structure shown in Fig. 6. These models do not use any variations at the lower boundary, so the extreme degree of clumping is entirely self-excited due to the rapid growth rate of the intrinsic instability. The lateral scale is limited only by the tiny scale (≅ $R/100$) of the Sobolev length, producing thousands of clumps in all.

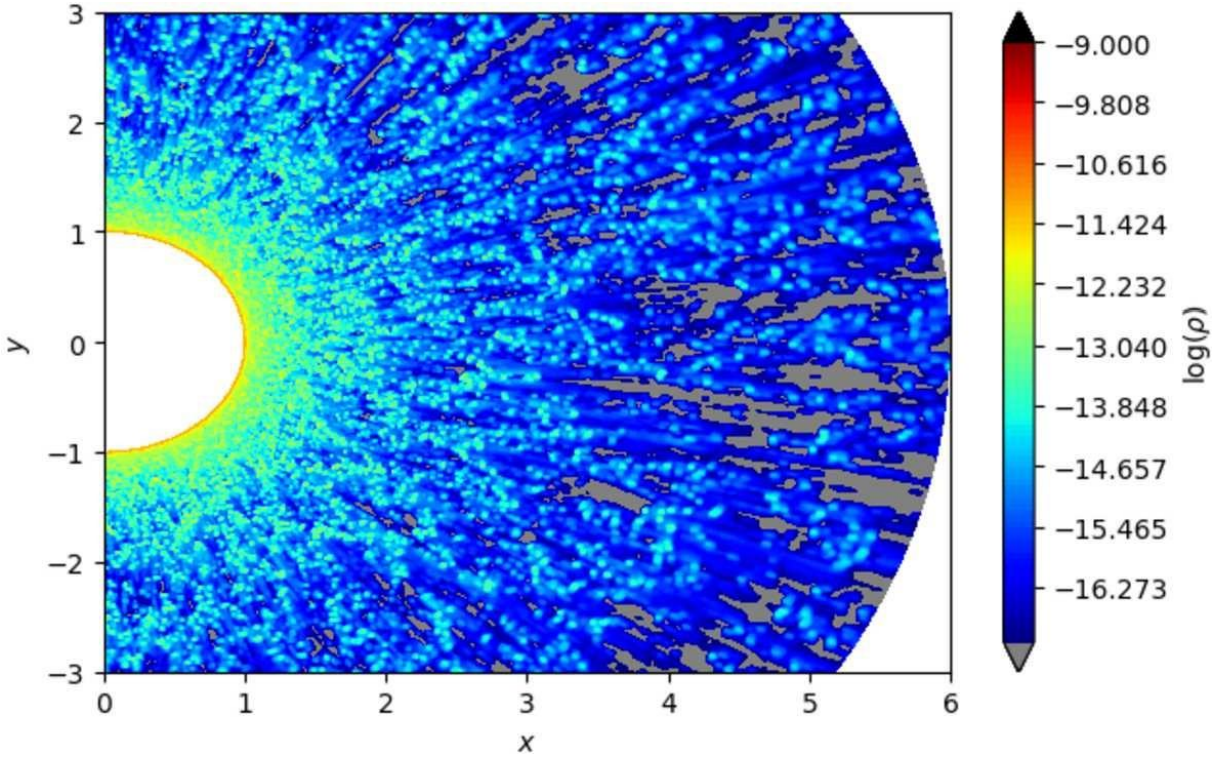

Fig. 6 Shown is the density structure in the 2D LDI simulation. To limit computing time, the radiative driving is entirely radial

As the radial scale is stretched out by the velocity instability, the clumps appear radially elongated. This causes absorption fluctuations that are wide in velocity (> 100 km s^{-1}), but spatially only a few percent of the radius, as can be seen in the time varying P Cygni profile in Fig. 7.

Published in : Astrophysics and Space Science (2022), vol. 367, n°123
DOI: 10.1007/s10509-022-04142-6
Status : Postprint (Author's version)

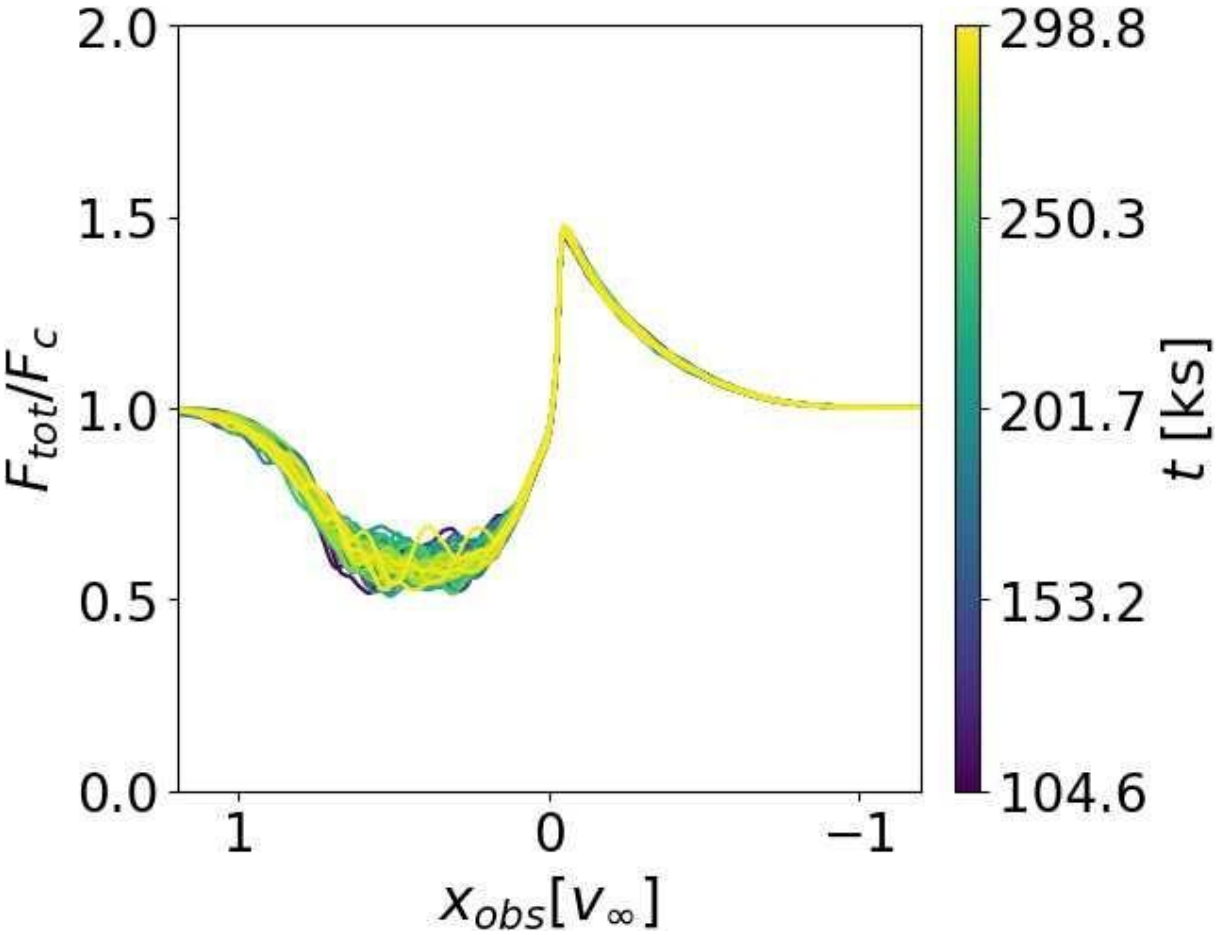

Fig. 7 Temporal snapshots of the P Cygni profile variations from the LDI simulation, showing variations of width > 100 km s^{-1}. The depth of the features is enhanced artificially in the 2D model by azimuthal coherence around the observer line of sight, and could be an order of magnitude less. The mean shape of the P Cygni absorption is less deep than a smooth model, owing to the effects of vorosity/porosity

Since the model is only 2D, there is an artificial azimuthal symmetry around the line to the observer, which produces circularly coherent structures that overestimate the magnitude of the variances shown. Assuming the azimuthal coherence length should actually be on the Sobolev scale, $\cong R/100$, an order of magnitude of cancellation in the temporal variations could be expected. This will require further modeling to explore, but given that the largest features have a variance approaching 10% in this azimuthally symmetric treatment, the largest temporal variations might appear at the 1% level or less. Thus it is important that the *Polstar* experiment described above achieves SNR in the range 400–1000, depending on the target brightness, so temporal variations over a day-long observation could easily characterize variances at the 1%level, or less. The intended binning to 20 km $^{s-1}$ resolution will also easily resolve the model features, which typically show a velocity width > 100 km s^{-1}.

The dynamical spectrum produced by this model is shown in Fig. 8. Again the artificial azimuthal coherence in the model may overestimate the amplitude of the features, but their general attributes are seen to be highly reminiscent of observed dynamic spectra. The model features have an acceleration that is seen to be nearly constant, and somewhat faster than what has been so far

Published in : Astrophysics and Space Science (2022), vol. 367, n°123
DOI: 10.1007/s10509-022-04142-6
Status : Postprint (Author's version)

observed. This may be because observed features are primarily limited to large DACs that may be linked to CIRs induced by rotating surface features such as spots, not the intrinsic wind features simulated here.

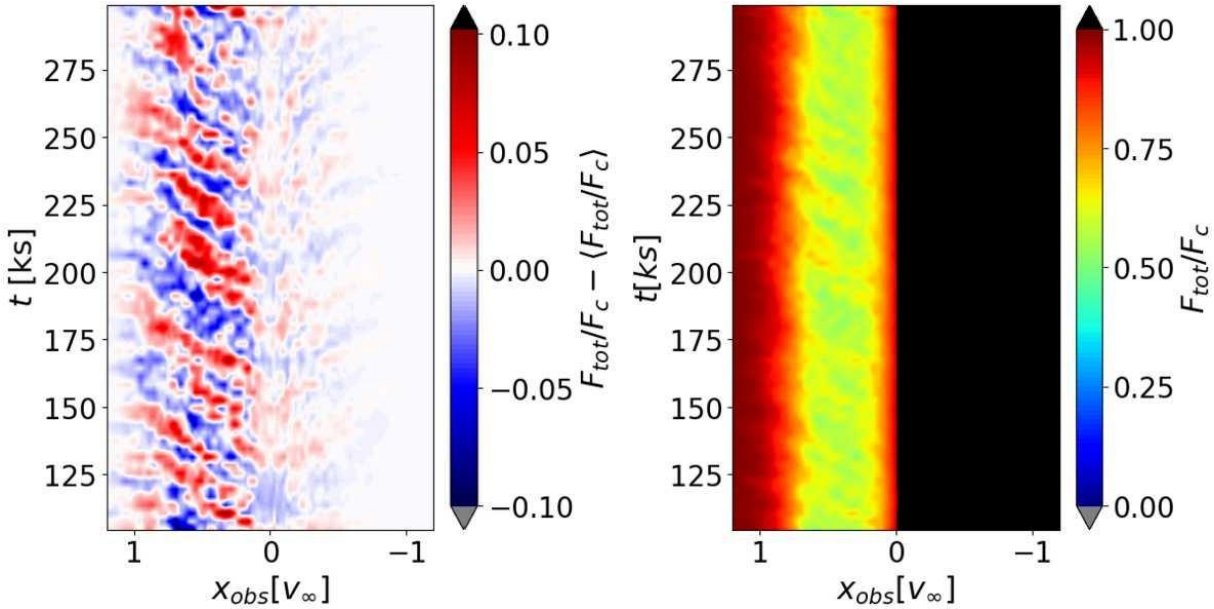

Fig. 8 Dynamic spectra from the LDI model are shown relative to the mean profile on the left, and for the full profile on the right. The velocity and temporal widths of the features are true to the simulation, but their magnitude is overestimated by perhaps an order of magnitude because of the model 2D azimuthal symmetry around the observer line of sight

A near-meter aperture such as *Polstar* allows a sufficiently high SNR to ascertain whether there are different acceleration rates for features linked to surface inhomogeneities, as opposed to self-excited clumps in the wind. If such potentially more rapid accelerations exist in the data, the wide features that appear in the simulation shown can still be temporally tracked using the exposure times in this experiment by binning the data to 100 km s^{-2}, approximately doubling the already high SNR in the process. Alternatively, if the accelerations are more at the scale of the surface gravity of the star, as may tend to be true of the few DACs that have been well resolved, then the finer binning at the sound speed level (≅20 km s^{-1}) will match well the exposure times and produce the experiment described in Sect. 3 above.

Also, the seeming quasi-periodicity seen in these simulations, despite including no rotation, allows for the possibility that the wind is "flapping" on its own intrinsic timescale. These day-long timescales might then be only coincidentally related to rotation periods of fast rotators like zeta Puppis, and the DACs might then be unrelated to spots or CIR features. This possibility can also be tested by *Polstar*, because enough stars will be targeted to include a range of inclinations and rotation rates. CIR-type structures would depend on those variables, but not intrinsic wind effects.

It should be noted that although these simulations include the LDI, they also involved physically motivated boundary conditions that are conducive to surface variations from the "nodal topology" of the line-driven critical point (Sundqvist and Owocki 2013). Hence, it is not yet clear if the features

Published in : Astrophysics and Space Science (2022), vol. 367, n°123
DOI: 10.1007/s10509-022-04142-6
Status : Postprint (Author's version)

seen in these simulations develop in the wind due to the instability, or propagate from the surface due to the nonlinearity of the driving.

Finally, the fact that observed DACs must cover a significant fraction of the stellar disk (in order to produce such deep features) presents challenges to every one of these models. With an order of magnitude improvement in SNR over the IUE MEGA campaign, *Polstar* will be able to search for a hierarchy of smaller structures that cover less of the stellar disk, to place the more dramatic DAC structures into a fuller context of other features that will help ascertain their true nature.

7. Conclusions

This paper summarizes many of the ways in which a dedicated space-borne UV spectropolarimeter, such as *Polstar*, could be used in the context of high resolution continuous observations of massive stars, to characterize nonspherical and inhomogeneous wind structures. The goals would be to better understand the wind dynamics, and provide more accurate determinations of the stellar mass-loss rates. This would be accomplished via a sequence of exposures, short enough (∼10 minutes) to track weak features as they move through the narrow resolution elements (∼ 10 km s^{-1}) in a series of UV resonance and excited-state line profiles within the UV band of the instrument. Effective areas in the range 30–100 cm^2 are sufficient to yield spectroscopic *SNR* > 400 at high resolution, and polarimetric *SNR* > 10, 000 at much lower resolution in both wavelength and time, for dozens of bright targets.

Such an unparalleled dataset could inform corrections of mass-loss rate determinations that are sensitive to density inhomogeneity, such as Hα and free-free radio emission. This would be informed by resolving moving features, and also by fitting the time-averaged line profile to account for enhanced escape of line photons through regions of low density (porosity), and their concomitant high velocity gradients (vorosity). This will lead to more accurate determinations of mass loss from high-mass main-sequence stars and blue supergiants, setting the stage for, and significantly altering, later evolutionary phases for single stars and binaries. In the process, the physics of the driving of these winds will be better understood, including the role of the LDI, surface perturbations including spots, and CIR-type structures modulated by stellar rotation.

AUTHOR CONTRIBUTION

All authors contributed to the writing of the paper. SE computed the evolutionary tracks in the *r-q* diagram presented in Sect. 2 and shown in Fig. 1. GJP and KGG were the main contributors to Sects. 2 and 3. RI and JLH primarily contributed the calculations and text for Sect. 4. GJP wrote Sect. 5.

FUNDING

RI acknowledges support from a grant by the National Science Foundation, AST-2009412. PS acknowledges support by the NASA Goddard Space Flight Center to formulate the mission proposal

Published in : Astrophysics and Space Science (2022), vol. 367, n°123
DOI: 10.1007/s10509-022-04142-6
Status : Postprint (Author's version)

for *Polstar*. YN acknowledges support from the Fonds National de la Recherche Scientifique (Belgium), the European Space Agency (ESA) and the Belgian Federal Science Policy Office (BELSPO) in the framework of the PRODEX Programme (contracts linked to XMMNewton and Gaia). SE acknowledges the STAREX grant from the ERC Horizon 2020 research and innovation programme (grant agreement No. 833925), and the COST Action ChETEC (CA 16117) supported by COST (European Cooperation in Science and Technology). A.D.- U. is supported by NASA under award number 80GSFC21M0002.

AuD acknowledges support by NASA through Chandra Award number TM1-22001B issued by the Chandra X-ray Observatory 27 Center, which is operated by the Smithsonian Astrophysical Observatory for and on behalf of NASA under contract NAS8-03060. NS acknowledges support provided by NAWA through grant number PPN/SZN/2020/1/00016/U/DRAFT/00001/U/00001. LH, FAD, and JOS acknowledge support from the Odysseus program of the Belgian Research Foundation Flanders (FWO) under grant G0H9218N. The authors also wish to thank the anonymous referee for several helpful suggestions, including adjustments of the target list.

DATA AVAILABILITY

Data sharing is not applicable to this article as no datasets were generated or analysed during the current study.

Declarations

STATEMENTS & DECLARATIONS

This research has made use of NASA's Astrophysics Data System and the SIMBAD database, operated at CDS, Strasbourg, France. The work has also made use of the BeSS database, operated at LESIA, Observatoire de Meudon, France: http://basebe.obspm.fr. This research made use of Astropy, http://www.astropy.org a community-developed core Python package.

COMPETING INTERESTS

The authors have no relevant financial or non-financial interests to disclose.

References

Andersson, B.G., Clayton, G.C., Doney, K.D., Panopoulou, G.V., Hoang, T., Magalhaes, A.M., Yan, H., Ignace, R., Scowen, P.A.: Ultraviolet spectropolarimetry with *Polstar*: interstellar medium science. Astrophys. Space Sci. **367** (2022). https://doi.org/10.1007/s10509-022-04153-3

Published in : Astrophysics and Space Science (2022), vol. 367, n°123
DOI: 10.1007/s10509-022-04142-6
Status : Postprint (Author's version)

Aurière, M., Wade, G.A., Silvester, J., et al.: Astron. Astrophys. **475**, 1053 (2007). https://doi.org/10.1051/0004-6361:20078189

Babel, J., Montmerle, T.: Astron. Astrophys. **323**, 121 (1997)

Balona, L.A.: Mon. Not. R. Astron. Soc. **490**, 2112 (2019). https://doi.org/10.1093/mnras/stz2808

Bouret, J.C., Lanz, T., Hillier, D.J., et al.: Astrophys. J. **595**, 1182 (2003). https://doi.org/10.1086/377368

Bowman, D.M., Burssens, S., Simon-Diaz, S., Edelmann, P.D.F., Rogers, T.M., Horst, L., Rofke, F.K., Aerts, C.: Astron. Astrophys. **640**, 36 (2020). https://doi.org/10.1051/0004-6361/202038224

Cantiello, M., Braithwaite, J.: Astron. Astrophys. **534**, A140 (2011). https://doi.org/10.1051/0004-6361/201117512

Cantiello, M., Langer, N., Brott, I., et al.: Astron. Astrophys. **499**, 279 (2009). https://doi.org/10.1051/0004-6361/200911643

Castor, J.I., Abbott, D.C., Klein, R.I.: Astrophys. J. **195**, 157 (1975). https://doi.org/10.1086/153315

Cranmer, S.R., Owocki, S.P.: Astrophys. J. **462**, 469 (1996). https://doi.org/10.1086/177166

Cranmer, S.R., Smith, M.A., Robinson, R.D.: Astrophys. J. **537**, 433 (2000). https://doi.org/10.1086/309008

David-Uraz, A.,Wade, G.A., Petit, V., et al.: Mon. Not. R. Astron. Soc. **444**, 429 (2014). https://doi.org/10.1093/mnras/stu1458

David-Uraz, A., Owocki, S.P.,Wade, G.A., Sundqvist, J.O., Kee, N.D.: Mon. Not. R. Astron. Soc. **470**, 3672 (2017). https://doi.org/10.1093/mnras/stx1478

Davies, B., Oudmaijer, R.D., Vink, J.S.: Astron. Astrophys. **439**, 1107 (2005). https://doi.org/10.1051/0004-6361:20052781

de Jong, J.A., Henrichs, H.F., Schrijvers, C., et al.: Astron. Astrophys. **345**, 172 (1999)

Dessart, L.: Astron. Astrophys. **423**, 693 (2004). https://doi.org/10.1051/0004-6361:20040543

Driessen, F.A., Kee, N.D., Sundqvist, J.O.: (2021). https://arxiv.org/abs/2110.05302

Feldmeier, A., Puls, J., Pauldrach, A.W.A.: Astron. Astrophys. **322**, 878 (1997)

Fullerton, A.W., Gies, D.R., Bolton, C.T.: Astrophys. J. Suppl. Ser. **103**, 475 (1996). https://doi.org/10.1086/192285

Fullerton, A.W., Massa, D.L., Prinja, R.K.: Astrophys. J. **637**, 1025 (2006). https://doi.org/10.1086/498560

Grunhut, J.H., Wade, G.A., Neiner, C., et al.: Mon. Not. R. Astron. Soc. **465**, 2432 (2017). https://doi.org/10.1093/mnras/stw2743

Hamann, W.R., Koesterke, L.: Astron. Astrophys. **335**, 1003 (1998)

Published in : Astrophysics and Space Science (2022), vol. 367, n°123
DOI: 10.1007/s10509-022-04142-6
Status : Postprint (Author's version)

Hamann, W.R., Brown, J.C., Feldmeier, A., Oskinova, L.M.: Astron. Astrophys. **378**, 946 (2001). https://doi.org/10.1051/0004-6361:20011253

Heap, S.R.: Astrophys. Space Sci. **221**, 87 (1994)

Hillier, D.J.: Astron. Astrophys. **247**, 455 (1991)

Howarth, I.D., Prinja, R.K.: Astrophys. J. Suppl. Ser. **69**, 527 (1989). https://doi.org/10.1086/191321

Jermyn, A.S., Cantiello, M.: Astrophys. J. **900**, 113 (2020). https://doi.org/10.3847/1538-4357/ab9e70

Kaper, L., Henrichs, H.F., Nichols, J.S., et al.: Astron. Astrophys. Suppl. Ser. **116**, 257 (1996)

Kaper, L., Henrichs, H.F., Fullerton, A.W., et al.: Astron. Astrophys. **327**, 281 (1997)

Lamers, H.J.G.L.M., Leitherer, C.: Astrophys. J. **412**, 771 (1993)

Langer, N.: Annu. Rev. Astron. Astrophys. **50**, 107 (2012). https://doi.org/10.1146/annurev-astro-081811-125534

Lecoanet, D., Cantiello, C., Quataert, E., Couston, L.-A., Burns, K.J., Pope, B.J.S., Jermyn, A.S., Favier, B., Le Bars, M.: Astrophys. J. **886**, 15 (2019). https://doi.org/10.3847/2041-8213/ab5446

Lépine, S., Moffat, A.F.J.: Astrophys. J. **514**, 909 (1999). https://doi.org/10.1086/306958

Massa, D., Prinja, R.K.: Astrophys. J. **809**, 12 (2015). https://doi.org/10.1088/0004-637X/809/1/12

Massa, D., Fullerton, A.W., Nichols, J.S., et al.: Astrophys. J. Lett. **452**, L53 (1995). https://doi.org/10.1086/309707

Massa, D., Oskinova, L., Prinja, R.: Astrophys. J. **873**, 81 (2019). https://doi.org/10.3847/1538-4357/ab0283

Michaud, G., Dupuis, J., Fontaine, G., Montmerle, T.: Astrophys. J. **322**, 302 (1987). https://doi.org/10.1086/165726

Moffat, A.F.J., Drissen, L., Lamontagne, R., Robert, C.: Astrophys. J. **334**, 1038 (1988). https://doi.org/10.1086/166895

Mokiem, M.R., de Koter, A., Evans, C.J., et al.: Astron. Astrophys. **465**, 1003 (2007). https://doi.org/10.1051/0004-6361:20066489

Momany, Y., Zaggia, S., Montalto, M., et al.: Nat. Astron. **4**, 1092 (2020). https://doi.org/10.1038/s41550-020-1113-4

Morton, D.C.: Astrophys. J. **203**, 386 (1976). https://doi.org/10.1086/154090

Mullan, D.J.: Astron. Astrophys. **165**, 157 (1986)

Nichols, J.S., Nazé, Y., Huenemoerder, D.P., Moffat, A.F.J., Miller, N.A., Lauer, J., Ignace, R., Gayley, K., Ramiaramanantsoa, T., Oskinova, L., Hamann, W.R., Richardson, N.D., Waldron, W.L., Dahmer, M.: Astrophys. J. **906**, 89 (2021). https://doi.org/10.3847/1538-4357/abca3a

Oskinova, L.M.: Adv. Space Res. 58, 7390 (2016)

Published in : Astrophysics and Space Science (2022), vol. 367, n°123
DOI: 10.1007/s10509-022-04142-6
Status : Postprint (Author's version)

Oskinova, L.M., Clarke, D., Pollock, A.M.T.: Astron. Astrophys. 378, L21 (2001). https://doi.org/10.1051/0004-6361:20011222

Oskinova, L.M., Hamann, W.R., Feldmeier, A.: Astron. Astrophys. 476, 1331 (2007). https://doi.org/10.1051/0004-6361:20066377

Owocki, S.P., Sundqvist, J.O.: Mon. Not. R. Astron. Soc. 475, 814 (2018). https://doi.org/10.1093/mnras/stx3225

Owocki, S.P., Castor, J.I., Rybicki, G.B.: Astrophys. J. 335, 914 (1988). https://doi.org/10.1086/166977

Petit, P., Hébrard, E.M., Böhm, T., Folsom, C.P., Lignières, F.: Mon. Not. R. Astron. Soc. **472**, L30 (2017). https://doi.org/10.1093/mnrasl/slx132

Prinja, R.K.: Mon. Not. R. Astron. Soc. **231**, 21P (1988). https://doi.org/10.1093/mnras/231.1.21P

Prinja, R.K., Howarth, I.D., Henrichs, H.F.: Astrophys. J. **317**, 389 (1987). https://doi.org/10.1086/165285

Prinja, R.K., Barlow, M.J., Howarth, I.D.: Astrophys. J. **361**, 607 (1990). https://doi.org/10.1086/169224

Puls, J., Kudritzki, R.P., Herrero, A., et al.: Astron. Astrophys. **305**, 171 (1996)

Puls, J., Markova, N., Scuderi, S., et al.: Astron. Astrophys. **454**, 625 (2006). https://doi.org/10.1051/0004-6361:20065073

Puls, J., Vink, J.S., Najarro, F.: Astron. Astrophys. Rev. **16**, 209 (2008). https://doi.org/10.1007/s00159-008-0015-8

Ramiaramanantsoa, T., Moffat, A.F.J., Chené, A.-N., et al.: Mon. Not. R. Astron. Soc. **441**, 910 (2014). https://doi.org/10.1093/mnras/stu619

Ramiaramanantsoa, T., Moffat, A.F.J., Harmon, R., et al.: Mon. Not. R. Astron. Soc. **473**, 5532 (2018). https://doi.org/10.1093/mnras/stx2671

Rauw, G., Hervé, A., Nazé, Y., González-Pérez, J.N., Hempelmann, A., Mittag, M., Schmitt, J.H.M.M., Schröder, K.-P., Gosset, E., Eenens, P., Uuh-Sonda, J.M.: Astron. Astrophys. **580**, A59 (2015). https://doi.org/10.1051/0004-6361/201526057

Robert, C., Moffat, A.F.J., Bastien, P., Drissen, L., St.-Louis, N.: Astrophys. J. **347**, 1034 (1989). https://doi.org/10.1086/168194

Schultz, W., Bildsten, L., Jiang, Y.-F.: Astrophys. J. **902**, 67 (2020). https://doi.org/10.3847/1538-4357/abb405

Scowen, P.A., Gayley, K.G., Ignace, R., Neiner, C., Vasudevan, G., Woodruff, R., Casini, R., Shultz, M.E., Andersson, B.G., Wisniewski, J.P.: The *Polstar* high resolution spectropolarimetry MIDEX mission. Astrophys. Space Sci. **367** (2022). https://doi.org/10.1007/s10509-022-04107-9

Shultz, M.E., Casini, R., Cheung, M.C.M., David-Uraz, A., del Pino Alemán, T., Erba, C., Folsom, C.P., Gayley, K.G., Ignace, R., Keszthelyi, Z., Kochukhov, O., Nazé, Y., Neiner, C., Oksala, M., Petit, V.,

Published in : Astrophysics and Space Science (2022), vol. 367, n°123
DOI: 10.1007/s10509-022-04142-6
Status : Postprint (Author's version)

Scowen, P.A., Sudnik, N., ud-Doula, A., Vink, J.S.,Wade, G.A.: Ultraviolet spectropolarimetry with *Polstar*: using *Polstar* to test magnetospheric mass-loss quenching. Astrophys. Space Sci. **367** (2022). https://doi.org/10.1007/s10509-022-04113-x

Snow, T.P. Jr., Morton, D.C.: Astrophys. J. Suppl. Ser. **32**, 429 (1976). https://doi.org/10.1086/190404

Sundqvist, J.O., Owocki, S.P.: Mon. Not. R. Astron. Soc. **428**, 1837 (2013). https://doi.org/10.1093/mnras/sts165

Sundqvist, J.O., Puls, J.: Astron. Astrophys. **619**, A59 (2018). https://doi.org/10.1051/0004-6361/201832993

Sundqvist, J.O., Owocki, S.P., Puls, J.: Astron. Astrophys. **611**, A17 (2018). https://doi.org/10.1051/0004-6361/201731718

Šurlan, B., Hamann, W.R., Aret, A., et al.: Astron. Astrophys. **559**, A130 (2013). https://doi.org/10.1051/0004-6361/201322390

ud-Doula, A., Owocki, S.P.: Astrophys. J. **576**, 413 (2002). https://doi.org/10.1086/341543

Vink, J.S., de Koter, A., Lamers, H.J.G.L.M.: Astron. Astrophys. **369**, 574 (2001). https://doi.org/10.1051/0004-6361:20010127